

Continuous generation of confined bubbles: viscous effect on the gravito-capillary pinch off

Haruka Hitomi¹ and Ko Okumura^{1*}

Physics Department and Soft Matter Center,

Ochanomizu University, 2-1-1 Ohtsuka,

Bunkyo-ku, Tokyo 112-8610, Japan

(Dated: June 17, 2025)

Abstract

We investigate continuous generation of bubbles from a bath of air in viscous liquid in a confined geometry. In our original setup, bubbles are spontaneously generated by virtue of buoyancy and a gate placed in the cell: the gate acts like an inverted funnel trapping air beneath it before continuously generating bubbles at the tip. The dynamics is characterized by the bubble-formation period and the bubble size as a function of the amount of air under the gate. By analyzing the data obtained for various parameters, we clearly identified that the dynamics of the bubble formation is governed by dissipation in the viscous fluid beneath the trapped air balanced by a gravitational energy change due to buoyancy, after examining numerous possibilities of dissipation, which demonstrates the potential of scaling analysis even in complex cases. Furthermore, we uncover a novel type of pinch-off condition, which convincingly explains the bubble size: in the present case viscosity plays a vital role, different from the conventional mechanism of Tate, in which gravity competes with capillarity, revealing a general mechanism of pinching-off at low Reynolds number. Accordingly, the present study significantly and fundamentally advances our knowledge of generation and pinch-off of bubbles, with the results relevant for a wide variety of applications in many fields. In particular, the present study demonstrates a promising avenue in microfluidics for understanding physical principles by scaling up the system, without losing the characteristics of the flow at low Reynolds numbers.

Drop and bubble formation at the end of a tube has been the subject of active investigations for a long time not only from fundamental but also from applicational interests in drop and bubbles [1], which includes oil recovery [2], soft electronics [3], cell therapy [4] and energy harvesting [5]. As early as in 1864, Tate discussed a pendant drop at the tip of a tube starts falling when its weight surpasses the capillary force supporting the weight [6], which remains a fundamental method to measure surface tension [7, 8]. A technically more sophisticated modern version of Tate, the continuous generation of droplets becomes increasingly important in microfluidics [9–14] due to recent demand for the manipulation of small amounts of liquids in various fields such as medicine, biochemistry, and pharmaceutical industries. However, basic physical principles governing the dynamics of the droplets formation at small scales and/or at low Reynolds numbers have yet to be elucidated. One of the difficulties in tackling this problem in microfluidics is the smallness of the system. One possible strategy to cope with this difficulty might be to use highly viscous liquid on centimeter scale in confined space. By virtue of this strategy, we have unveiled a number of governing principles regarding drop and bubble dynamics in the form of scaling laws, focusing on viscous friction [15–18], coalescence [19–21], breakup [22, 23], and bursting [24]. In this study, we focus on the continuous formation of bubbles on centimeter scale in a confined geometry, which is much more directly relevant for microfluidics, to reveal physical principles governing the dynamics in the form of scaling laws. Using an original setup, we successfully obtained scaling laws through a clear data collapse with elucidating physical pictures behind the simple laws.

Salient features of the present study are as follows. (1) To provide an example of emergence of scaling laws from numerous possibilities of viscous dissipations; in other words, we have obtained a remarkably simple physics from a seemingly complex problem, demonstrating the power of scaling analysis. (2) To provide a condition of breakup in which viscous effect is crucial in addition to the conventional Tate’s mechanism of the balance of gravity and capillarity, revealing a novel and general mechanism of pinching-off. (3) To provide an example, in which physical principles relevant for microfluidics can be effectively elucidated by using a system on centimeter scale without losing the main character of the flow at low Reynolds numbers. The present results not only advance fundamental knowledge on drops and bubbles but also provide guiding principles relevant for numerous applications at low Reynolds numbers in various fields such as microfluidics and oil industry.

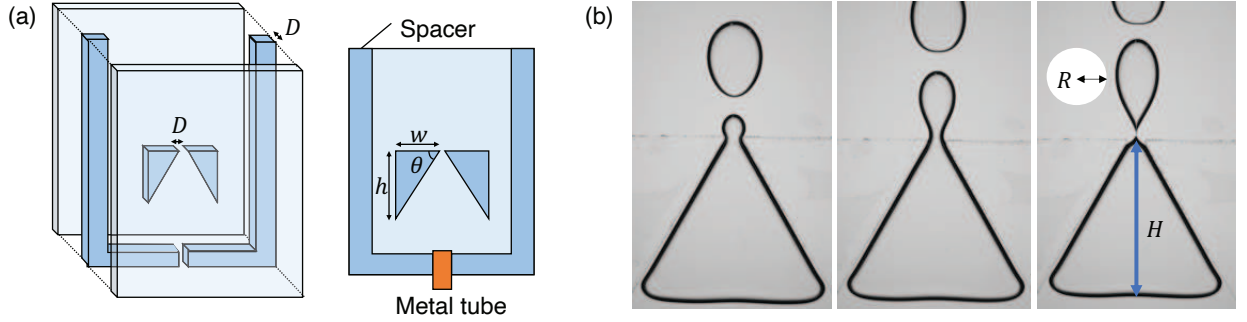


FIG. 1: (a) Experimental setup with a gate. (b) Continuous generation of bubbles observed in the cell for $(D, \theta, \nu) = (2, 60, 30)$ in mm, deg., and St, respectively. The radius R of the white circle having the same area with the bubble on the right characterizes the size of the bubble.

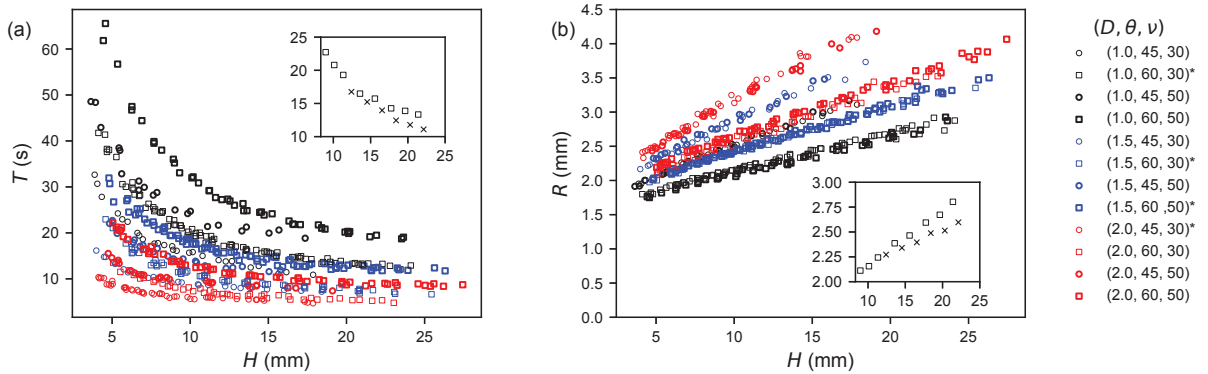


FIG. 2: (a) T vs H and (b) R vs H on linear scales. The insets demonstrate the existence of the region in which T and R bifurcate (or oscillate with H). See the text for further details. D and ν in the legend are given in mm and St, respectively (note that $30 \text{ St} = 3000 \text{ cSt}$).

In this experiment, we fabricate a thin cell sometimes called a Hele-Shaw cell (of thickness $D = 1.0$ to 2.0 mm, width 15 cm and height 20 cm) equipped with a gate (of width D and angle $\theta = 45$ to 60 deg.) and fill the cell with a viscous liquid (of kinematic viscosity $\nu = 3000$ to 5000 cSt), as in Fig. 1 (a). We inject air with a syringe through a brass tube (of inner radius 3.8 mm) at the bottom of the cell to observe a squashed chunk of air rising in the viscous liquid, which is trapped for a while under the gate with reducing its mass as a result of continuously generating bubbles, as in Fig. 1 (b). To characterize the dynamics, we measure the period of generation T and the characteristic size R ($\gg D$) of the bubble seen from front as a function of the height H of the air trapped under the gate [see the

rightmost photo of Fig. 1 (b)].

The density ρ and surface tension γ of the viscous liquid [polydimethylsiloxane (PDMS)] are 970 to 980 kg/m³ and $\gamma = 20$ mN/m, respectively. To prevent cell deformation due to capillary adhesion, we use 5mm-thick acrylic plates for $D = 1.0, 1.5$ mm and 2.0 mm-thick acrylic plates for $D = 2.0$ mm. In fact, the cell thickness D is precisely determined using the laser distance sensor (ZS-HLD2, Omron) and the precise value is used in the analysis, although, for simplicity, D is represented by approximate values (1.0, 1.5, or 2.0 mm) as above (differences are within 3%).

Since the bubble has a tear-drop shape (of area A) as seen in Fig. 1 (b), the characteristic size R is defined through the relation $A = \pi R^2$. The period of generation T for a bubble is defined as the time difference between the moment of pinch-off the bubble of our focus and that of the previous bubble. Similarly, H for a bubble of our focus is defined as the height at the moment of pinch-off of the previous bubble.

In Fig. 2 (a) and (b), we respectively show T and R as a function of H . The data marked with an asterisk (*) in the legend of Fig. 2 contain data obtained on different days, where cells were refabricated each day (those without asterisk are obtained within two hours using the same cell). We observe that the marked data sets match well with the other data, which demonstrates a reasonably good reproducibility of the experiment.

The insets shows that T and R as a function of H start bifurcating (or oscillating with H) as H decreases, where we analyze only the data on the upper branch (we do not use the data represented by the cross mark in the following). The reason of the bifurcation or oscillation is as follows. Due to the continuous bubble generation from air trapped under the gate, the volume of air under the gate (and thus H) keep decreasing, and the period of generation of bubbles T decreases with time (and thus with decrease in H). This implies that the distance between created bubbles becomes short with time. As a result, at certain point, the upwards flow caused by a bubble just created could start to affect the creation of the next bubble. If the n th bubble drags the $(n + 1)$ th bubble, which results in T and R in the lower branch (represented by the cross mark), then the $(n + 2)$ th bubble is no longer affected by the $(n + 1)$ th bubble. However, the $(n + 2)$ th bubble does drag the $(n + 3)$ th bubble. In this way, we observe the alternate bifurcation (or oscillation with H), where the $(n + 2m)$ th bubbles (with $m = 0, 1, 2, \dots$) are of our focus because the creation of them is

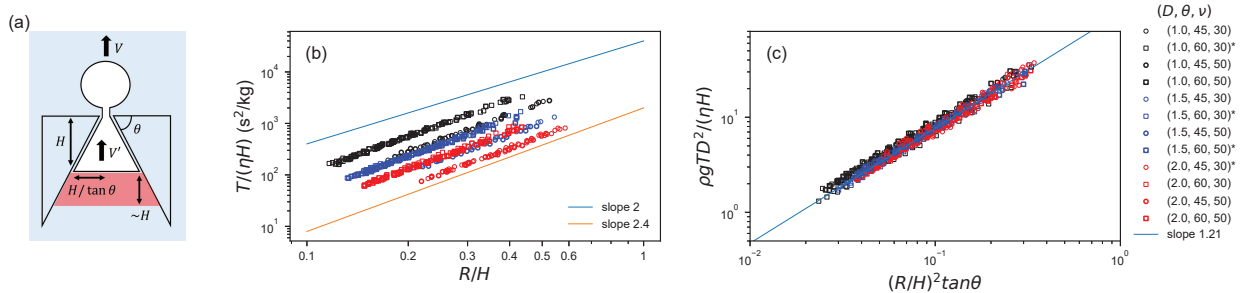


FIG. 3: (a) Physical picture for the dynamics: The dissipation in the liquid beneath the triangular air pocket trapped under the gate balances the gravitational energy change due to buoyancy. (b) $T/(\eta H)$ vs (R/H) on log-log scales, confirming Eq. (1). (c) $\rho g T D^2/(\eta H)$ vs $(R/H)^2 \tan \theta$ on log-log scales, confirming the physical picture in (a), i.e., Eq. (3).

completed without the drag effect of the previous bubble.

Figure 3 explains the relation between T as a function of H with the illustration in (a) summarizing the physical picture: the dynamics is determined by the balance between the gravitational energy change due to buoyancy and viscous dissipation in the viscous liquid beneath the large triangular air pocket trapped under the gate.

To justify this explanation, we first confirm that the plot in Fig. 3 (b) clearly support the relation

$$T/(\eta H) = k(D, \theta)(R/H)^{2\alpha} \quad (1)$$

with $\alpha \simeq 1.2$, where the coefficient k is dependent on D and θ . This is understood as follows. In the plot, colors and symbols respectively distinguish D and θ , while ν is distinguished by the thickness of the outline of a symbol. We observe in the plot the data with the same color and symbol collapse onto a straight line, while if the color or/and symbol are different the corresponding data collapse onto a shifted straight line with the same slope. In this observation, the universal slope corresponds to 2α in Eq. (1) and the shift reflects the dependence of k on D and θ . If we further note that the data with the same color and symbol collapse onto the same straight line even if the thickness are different, we can understand k is independent from ν . In this way, we can confirm Eq. (1) in Fig. 3 (b).

Second, we consider numerous possibilities of dissipation balanced with the energy change due to buoyancy, as explained in detail in Fig. 5 below. In this consideration, Eq. (1) is very helpful, since if a possibility of dissipation does not lead to a result that is consistent

with Eq. (1) we can exclude the possibility as not playing a dominant role. In other words, Eq. (1) gives a restriction on the possibility. Remarkably, this restriction is very sever and we find that only one single possibility is consistent with Eq. (1).

This only possibility is illustrated in Fig. 3 (a), where the large triangular air pocket under the gates is moving upwards with a velocity V' . This velocity can be estimated from a volume conservation as $V'T(2H/\tan\theta)D = \pi R^2D$, which can be expressed as

$$V \sim V'H/(R\tan\theta) \text{ with } R \sim VT, \quad (2)$$

and necessarily induces a velocity gradient $\sim V'/D$ inside the viscous fluid in the vicinity of the bottom of the air pocket in a volume $\sim DH^2/\tan\theta$, comparable to the volume of the triangular air pocket, as indicated in the illustration. We balance the dissipation energy during the time T (i.e. during the creation of one bubble) with the corresponding change in gravitational energy: $\rho gR^2DH \simeq T\eta(V'/D)^2(H^2/\tan\theta)D$. From the volume conservation and energy balance, we obtain

$$\rho gTD^2/(\eta H) \simeq (R/H)^2 \tan\theta, \quad (3)$$

which is in accord with Eq. (1): $k(D, \theta) \simeq \tan\theta/(\rho gD^2)$ and $\alpha \simeq 1$.

This relation is convincingly confirmed by a clear collapse of data shown in Fig. 3 (c) without any fitting parameters, although the agreement is not perfect. The slope (α) of the straight line in (c) obtained by numerical fitting is $\alpha = 1.21 \pm 0.04$, which is slightly larger than the expected value of $\alpha = 1$.

Strictly speaking, the bubble and air pocket are both covered with lubricating films (of thickness h) of the viscous fluid, which implies that there is no direct contact of air with the surface of the cell plates. However, we expect this thickness is very thin and for simplicity we assumed $D \gg h$, in the above and the ensuing discussion (a quantitative justification is also possible, as given below).

Figure 4 explains the relation between R as a function of H with the illustration in (a) summarizing a surprising physical picture: buoyancy opposed not only by capillarity but also by viscosity determines the condition of pinch-off, different from Tate's law. If we consider a natural form of viscous stress $\eta V/D$ acting on the circumference of the disk-shaped bubble whose area scales as RD , we obtain a force balance

$$\rho gR^2D = \alpha\gamma D + \beta\eta VR \quad (4)$$

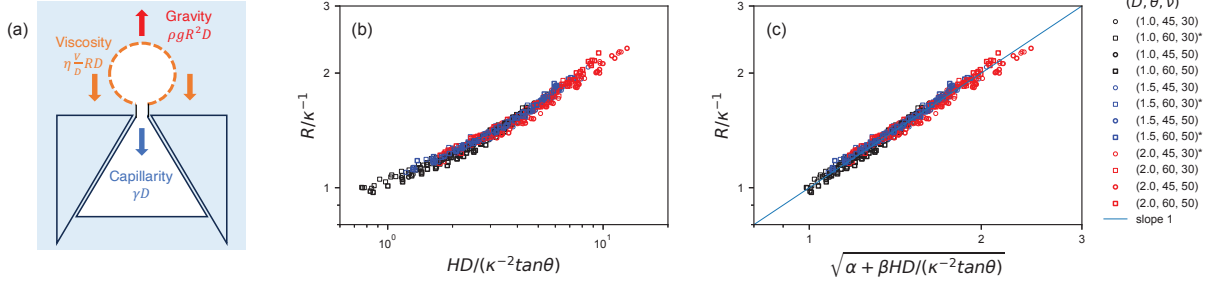


FIG. 4: (a) Physical picture for pinch-off: Buoyancy is opposed by viscosity in addition to capillarity. (b) R/κ^{-1} vs $HD/\tan\theta$ on log-linear scales, confirming Eq. (5) without any fitting parameter. (c) R/κ^{-1} vs $\sqrt{\alpha + \beta HD/(\kappa^{-2} \tan\theta)}$ on linear scales, demonstrating an excellent agreement, with using the result of fitting for α and β specified in the text.

with dimensionless coefficients α and β . To remove V from this equation, we use an equation for the bubble velocity $R \simeq VT$ and Eq. (3) for T , we arrive at the following relation based on the unexpected pinch-off condition with the capillary length $\kappa^{-1} = \sqrt{\gamma/(\rho g)}$:

$$R/\kappa^{-1} = \sqrt{\alpha + \beta HD/(\kappa^{-2} \tan\theta)} \quad (5)$$

This equation reveals that the dimensionless quantity R/κ^{-1} should be a function of a dimensionless quantity $HD/(\kappa^{-2} \tan\theta)$, which is convincingly confirmed in Fig. 4 (b) without any fitting parameters. We further use Eq. (5) to fit the data to obtain $\alpha = 0.665 \pm 0.04$ and $\beta = 0.411 \pm 0.02$ by taking averages of numerical fitting for each parameter. An excellent agreement between this result of fitting and the data is shown in Fig. 4 (c).

The collapse seen in Fig. 4 (b), or Eq. (5), suggests that R is independent from η . This is consistent with the balance in Eq. (4), in which the last term describing the shear stress is in fact independent of η , as encountered in Poiseuille flow in a pipe: The shear stress $\eta VR \sim \eta R^2/T$ is independent from η , because T is proportional to η , as suggested by the collapse in Fig. 3 (c), or Eq. (3).

Although we focus on the conditions at the pinch off in the above scaling arguments, we can discuss some dynamical picture leading to the pinch off. Just after a pinch off, the triangular air pocket of height H starts to push a new bubble through the orifice, which is possible because the capillary force at the orifice $\simeq \gamma D$ is smaller than the buoyancy $\simeq \rho g D H^2 / \tan\theta$, i.e., $\kappa^{-1} < H$. Then the liquid below the bubble starts to move and viscous dissipation characterized by a velocity gradient V'/D starts building up beneath the

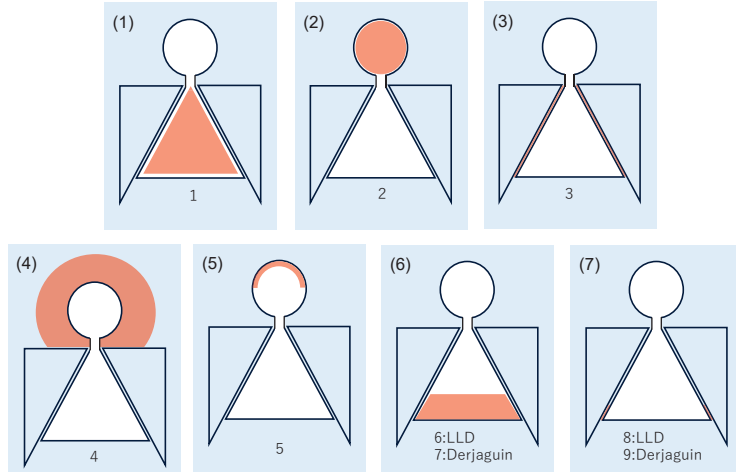


FIG. 5: Numerous possibilities of viscous dissipation considered in the present study. The red region indicates the place in which a velocity gradient is developed.

triangular air pocket of height H to reach a force balance $\rho g D H^2 / \tan \theta \simeq \eta (V'/D) H^2 / \tan \theta$ at the velocity

$$V' \simeq \rho g D^2 / \eta, \quad (6)$$

which is independent of H . From this expression for V' and the volume conservation in Eq. (2), we recover Eq. (3) previously obtained by an energy balance. To deepen the dynamical picture given above, we consider the governing forces acting on the growing bubble: the upward buoyancy $\sim \rho g R^2 D$ is opposed by the downward forces of viscous and capillary origins, $\sim \eta (V/D) R D$ and $\sim \gamma D$. Dynamically, while the last capillary force has a geometrical maximum, the upward buoyancy ($\sim R$) increases in magnitude and the downward viscous force, which can be expressed as $\rho g D^2 H$ using Eqs. (2) and (6), decreases. This dynamical balance implies that the buoyancy eventually becomes dominant leading to the pinch off, at which Eq. (4) is satisfied. Furthermore, the viscous force acting on the bubble, which eventually appears in Eq. (4), corresponds to a viscous dissipation per time around the bubble characterized by the velocity gradient V/D in a volume $R D^2$ (see Appendix A1). This dissipation can be shown to be smaller than the dissipation beneath the triangular pocket considered in deriving Eq. (3), from Eqs. (2) and (6), which supports the derivation of Eq. (3).

Throughout the present study, we ignored the effect of inertia, which is justified as follows. We can estimate the upper bound for Reynolds number by $Re = \eta V L / \eta$ once a relevant

characteristic length scale L is identified. Judging from Eqs. (3) and (5), it is natural to consider that L would scale as κ^{-1} , which is comparable with D . Then, considering the range of parameters in the present study, we confirmed Re is less than 0.0005 (for $L = 1.8$ mm), which means $Re \ll 1$, as we assumed. In the above, we used V instead of V' , which implies Re could be overestimated because $V > V'$. This guarantees that the above conclusion $Re \ll 1$ is valid even if this issue is taken into account.

We examine the validity of the assumption $D \gg h$. The thickness h of the lubricating film can be estimated by the theory of Landau, Levich, and Derjaguin (LLD) [25, 26] or that of Derjaguin [26, 27]: h can be respectively estimated as $h_{LLD} = 0.94\kappa^{-1}Ca^{2/3}$ and $h_D = \kappa^{-1}Ca^{1/2}$ with the capillary number $Ca = \gamma U/\eta$ for a characteristic velocity U , which suggests the use of V for U could give an overestimate for Ca . In the present study, if we estimate Ca with $U = V$, Ca is in the range from 0.00661 to 0.146, with the average 0.045 and the standard deviation 0.03, to confirm $Ca < 1$. Note that this conclusion $Ca < 1$ is valid even if we use $U = V'$ since $V > V'$. Based on the range of Ca thus obtained, the theory of Derjaguin predicts h/D to be in the range from 0.12 to 0.19 with the average 0.16 and the standard deviation 0.01, to reasonably well confirm $h/D \ll 1$. This conclusion $h/D \ll 1$ does not change even if we use $U = V'$ and/or LLD theory because both replacements could only lead to a smaller value of h/D (Note here $h_D \sim Ca^{1/2} > h_{LLD} \sim Ca^{2/3}$ if $Ca < 1$): the above estimate could be an overestimate for these two aspects (If $\kappa^{-1} \gtrsim D$ as in the present study, h_{LLD} and h_D could scale not with κ^{-1} but rather with D ; e.g., $h_D \sim DCa^{1/2}$; the above estimate based on $h_D = \kappa^{-1}Ca^{1/2}$ could be an overestimate even in this respect).

As announced previously, we considered various possibilities for dissipation other than the one considered in the above, as specified in Fig. 5 (1) to (7), where the region in which the velocity gradient is developed is suggested in red. In Fig. 5 (1) to (3), the dissipation in thin films is indicated. However, because of a low viscosity of air, even though air is moving, the air cannot drag the liquid surface effectively to induce a significant velocity gradient. For this reason, we exclude these three possibilities. In Fig. 5 (4), a velocity gradient $\sim V/D$ is developed around the bubble in a volume $\sim R^2D$ or $\sim RD^2$ (see Appendix A1). However, this dissipation does not give any θ dependence, which is inconsistent with Eq. (1), and thus is excluded. In Fig. 5 (5) to (7), velocity gradients developed inside the dynamic meniscus in thin films are considered. However, the case of Fig. 5 (5) again fails to give any θ dependence, and thus is excluded. The remaining cases of Fig. 5 (6) and (7) are also

excluded because we again fail to obtain the form consistent with Eq. (1) even though we have some θ dependence and even though we consider the two possibilities of $h = h_{LLD}$ and $h = h_D$ in each case, as shown in Appendix A2.

In this way, although we tested nine cases as suggested in Fig. 5, all were excluded: the only possibility is the one leading to Eq. (3). In other words, the present case is rather complex in that there are many possibilities for the region in which dissipation could occur. Despite this complexity, a governing dissipation is singled out from numerous possibilities to results in simple and clear scaling laws. In this sense, the present study is a remarkable example of a simple physics emerging from complexity.

In addition, the effect of viscosity on the Tate's condition of pinch-off uncovered in the present study should be a general mechanism to be considered in many other cases in microfluidics or/and at low Reynolds numbers. Together with this, the present study provides a clear and fundamental physical understanding for the dynamics of continuous bubble formation relevant for numerous applications, advancing and impacting on the field, demonstrating a system on centimeter scales could be useful.

Acknowledgments

We are grateful to an anonymous referee, who gave us deep and insightful comments, including those on the dynamical picture of the present pinch off. We thank Mana Iwasaki and Yuka Katsumata for contribution for initial stage of the present work. This work was supported by JSPS KAKENHI Grant Number JP19H01859 and JP24K00596.

-
- [1] A. Frohn and N. Roth. *Dynamics of Droplets*. Springer, Berlin, 2000.
 - [2] Saeed Shad, Majid Salarieh, Brij Maini, and Ian D Gates. The velocity and shape of convected elongated liquid drops in narrow gaps. *J. Petroleum Sci. Eng.*, 72(1):67–77, 2010.
 - [3] Wedyan Babatain, Min Sung Kim, and Muhammad Mustafa Hussain. From droplets to devices: Recent advances in liquid metal droplet enabled electronics. *Advanced Functional Materials*, 34(31):2308116, 2024.
 - [4] Hiroki Yasuga, Emre Iseri, Xi Wei, Kerem Kaya, Giacomo Di Dio, Toshihisa Osaki, Koki Kamiya, Polyxeni Nikolakopoulou, Sebastian Buchmann, Johan Sundin, et al. Fluid interfacial

- energy drives the emergence of three-dimensional periodic structures in micropillar scaffolds. *Nature Physics*, 17(7):794–800, 2021.
- [5] Wanghuai Xu, Huanxi Zheng, Yuan Liu, Xiaofeng Zhou, Chao Zhang, Yuxin Song, Xu Deng, Michael Leung, Zhengbao Yang, Ronald X Xu, et al. A droplet-based electricity generator with high instantaneous power density. *Nature*, 578(7795):392–396, 2020.
- [6] T. Tate. Xxx. on the magnitude of a drop of liquid formed under different circumstances. *The London, Edinburgh, and Dublin Philosophical Magazine and Journal of Science*, 27(181):176–180, 1864.
- [7] B Vinet, JP Garandet, and L Cortella. Surface tension measurements of refractory liquid metals by the pendant drop method under ultrahigh vacuum conditions: Extension and comments on tate’s law. *Journal of applied physics*, 73(8):3830–3834, 1993.
- [8] Joseph D Berry, Michael J Neeson, Raymond R Dagastine, Derek YC Chan, and Rico F Tabor. Measurement of surface and interfacial tension using pendant drop tensiometry. *Journal of colloid and interface science*, 454:226–237, 2015.
- [9] PB Umbanhowar, V Prasad, and David A Weitz. Monodisperse emulsion generation via drop break off in a coflowing stream. *Langmuir*, 16(2):347–351, 2000.
- [10] Shelley L Anna, Nathalie Bontoux, and Howard A Stone. Formation of dispersions using ‘flow focusing’ in microchannels. *Applied Physics Letters*, 82(3):364–366, 2003.
- [11] Andrew S Utada, Alberto Fernandez-Nieves, Howard A Stone, and David A Weitz. Dripping to jetting transitions in coflowing liquid streams. *Physical Review Letters*, 99(9):094502, 2007.
- [12] Gordon F Christopher and Shelly L Anna. Microfluidic methods for generating continuous droplet streams. *Journal of Physics D: Applied Physics*, 40(19):R319, 2007.
- [13] Shia-Yen Teh, Robert Lin, Lung-Hsin Hung, and Abraham P Lee. Droplet microfluidics. *Lab on a Chip*, 8(2):198–220, 2008.
- [14] Pingan Zhu and Liqiu Wang. Passive and active droplet generation with microfluidics: a review. *Lab on a Chip*, 17(1):34–75, 2017.
- [15] Ayako Eri and Ko Okumura. Viscous drag friction acting on a fluid drop confined in between two plates confined in between two plates. *Soft Matter*, 7:5648, 2011.
- [16] Misato Yahashi, Natsuki Kimoto, and Ko Okumura. Scaling crossover in thin-film drag dynamics of fluid drops in the hele-shaw cell. *Sci. Rep.*, 6:31395, 2016.
- [17] Mayuko Murano and Ko Okumura. Rising bubble in a cell with a high aspect ratio cross-

- section filled with a viscous fluid and its connection to viscous fingering. *Physical Review Research*, 2(1):013188, 2020.
- [18] Nana Tanaka and Ko Okumura. Viscous friction acting on a solid disk falling in confined fluid: Lessons for the scaling analysis. *Physical Review Research*, 5(3):L032047, 2023.
- [19] Ayako Eri and Ko Okumura. Bursting of a thin film in a confined geometry: Rimless and constant-velocity dewetting. *Phys. Rev. E*, 82(3):030601(R), Sep 2010.
- [20] Maria Yokota and Ko Okumura. Dimensional crossover in the coalescence dynamics of viscous drops confined in between two plates. *Proc. Nat. Acad. Sci. (U.S.A.)*, 108:6395–6398; In this issue, PNAS, 108 (2011) 6337., 2011.
- [21] Yukina Margaret Koga and Ko Okumura. Inertial coalescence of a liquid drop surrounded by viscous liquid. *Journal of the Physical Society of Japan*, 91(2):025001, 2022.
- [22] Hana Nakazato, Yuki Yamagishi, and Ko Okumura. Self-similar dynamics of air film entrained by a solid disk in confined space: A simple prototype of topological transitions. *Physical Review Fluids*, 3(5):054004, 2018.
- [23] Hana Nakazato and Ko Okumura. Air entrained into viscous liquid by a disk: Confinement induced suppression of breakup. *Physical Review Research*, 4(1):013150, 2022.
- [24] Mayuko Murano and Ko Okumura. Bursting dynamics of viscous film without circular symmetry: The effect of confinement. *Physical Review Fluids*, 3(3):031601, 2018.
- [25] L Landau and B Levich. *Physicochim. Acta. Physicochim (URSS)*, 17:42, 1942.
- [26] B.V. Derhaguin. *Doklady AN S.S.S.R.*, 11:39, 1943.
- [27] BVCR Derjaguin. On the thickness of the liquid film adhering to the walls of a vessel after emptying. *Progress in Surface Science*, 43(1-4):134–137, 1993.

. APPENDIX

A1. Dissipation around the growing bubble

The present experimental data strongly suggest that the dissipation (per time) around the growing bubble is characterized by a velocity gradient $\sim V/D$ in a volume $\sim RD^2$ (not $\sim R^2D$), which can be shown to be smaller than the dissipation beneath the triangular air pocket as discussed in the text. This is understood from the shear force considered in Eq.

(4) $\sim \eta(V/D)RD$, which is transformed into dissipation energy per time by multiplying a factor $\sim V$: $\eta(V/D)^2RD^2$. This is in contrast with the dissipation per time around a rising bubble, which is not growing but has a fixed volume, in a Hele-Shaw cell, which is characterized by a velocity gradient $\sim V/D$ in a volume $\sim R^2D$ in previous studies (see [15] and references therein). Note that the shear force considered in Eq. (4) cannot be interpreted as $\sim \eta(V/R)R^2$ because it leads to the dissipation $\sim \eta(V/R)^2R^3$, which is rather for a three-dimensional bubble.

A2. Scaling arguments for the cases in Fig. 5 (6) and (7)

Before going into the specific cases, we slightly extend the theory of LLD and Derjaguin at the level of scaling laws, for a film of thickness h . In the film, a velocity gradient $\sim U/h$ is developed only in the region of dynamic meniscus whose length scale is characterized by l . The LLD theory is based on the Stokes equation and matching condition:

$$\eta \frac{U}{h^2} \sim \frac{1}{l} \frac{\gamma}{l_0} \text{ and } \frac{1}{l_0} \sim \frac{h}{l^2}. \quad (\text{A2.7})$$

In the first relation, the viscous stress balances with the pressure gradient originating from Laplace's pressure jump γ/l_0 . In the second, the radius of curvature l^2/h is matched with the length l_0 , which is the capillary length κ^{-1} in the original theory but here is replaced by the cell thickness D if $D \ll \kappa^{-1}$, where this replacement implies a slight extension of the original theory. From Eq. (A2.7), we obtain

$$l \sim l_0(\eta U/\gamma)^{1/3} \text{ and } h \sim l_0(\eta U/\gamma)^{2/3}, \quad (\text{A2.8})$$

In Derjaguin's theory, Eq. (A2.7) is replaced by

$$\eta \frac{U}{h^2} \sim \rho g \text{ and } \frac{1}{l_0} \sim \frac{h}{l^2}, \quad (\text{A2.9})$$

from which we obtain

$$l \sim (\kappa^{-1}l_0)^{1/2}(\eta U/\gamma)^{1/4} \text{ and } h \sim \kappa^{-1}(\eta U/\gamma)^{1/2}, \quad (\text{A2.10})$$

In Fig. 5 (6), we consider a velocity gradient $\sim U/h$ with $U = V'$ inside the film (thickness h) developed in the dynamic meniscus contacting on the surface of cell plates in a volume

$\sim hlH/\tan\theta$, which leads to the following gravity-viscous energy balance during the time comparable to T :

$$\rho g R^2 D H \sim T \eta (V'/h)^2 hlH/\tan\theta \quad (\text{A2.11})$$

If we use the LLD theory, this balance can be reduced in the following form in which the l_0 dependences are cancel out, by using Eq. (A2.8) with $U = V'$ together with the volume conservation $V'T(2H/\tan\theta)D = \pi R^2 D$:

$$\left(\frac{\rho g T D^2}{\eta H}\right)^2 \simeq \tan^2\theta \frac{\kappa^{-2} R^4 D}{H^7}, \quad (\text{A2.12})$$

which is not compatible with Eq. (1), and thus this case is excluded from possible candidates.

If we instead use Derjaguin theory, the energy balance in Eq. (A2.11) reduces to the following form, with the aid of Eq. (A2.10) with $U = V'$ together with the same volume conservation:

$$\left(\frac{\rho g T D^2}{\eta H}\right)^3 \simeq \tan^3\theta l_0^2 R^6 D^2 / H^{10}, \quad (\text{A2.13})$$

which is again not compatible with Eq. (1), and thus this case is also excluded.

In Fig. 5 (7), we consider a velocity gradient $\sim U/h$ with $U = V'/\sin\theta$ inside the film (thickness h) developed in the dynamic meniscus contacting on the surface of the gates in a volume $\sim hlD$, which lead to the following gravity-viscous energy balance during the time comparable to T :

$$\rho g R^2 D H \sim T \eta \left(\frac{V'}{h \sin\theta}\right)^2 hlD \quad (\text{A2.14})$$

If we use the LLD theory, this balance can be reduced in the following form in which the l_0 dependences are cancel out, by using Eq. (A2.8) with $U = V'/\sin\theta$ together with the same volume conservation $V'T(2H/\tan\theta)D = \pi R^2 D$:

$$\left(\frac{\rho g T D^2}{\eta H}\right)^2 \simeq \frac{\kappa^{-2} R^4 D^4}{H^{10} \cos^5\theta}, \quad (\text{A2.15})$$

which is not compatible with Eq. (1), and thus this case is excluded from possible candidates.

If we instead use Derjaguin theory, Eq. (A2.14) reduces to the following form, with the aid of Eq. (A2.10) with $U = V'/\sin\theta$ together with the same volume conservation:

$$\left(\frac{\rho g T D^2}{\eta H}\right)^3 \simeq \frac{l_0^2 R^6 D^6}{H^{14} \cos^7\theta}, \quad (\text{A2.16})$$

which is again not compatible with Eq. (1), and thus this case is also excluded.

In this way, even though we considered four cases corresponding to Fig. 5 (6) and (7), all the cases are not in the form of Eq. (1) and thus are excluded.